Article

Determination of the Elastic Moduli of a Single Cell Cultured on a Rigid Support by Force Microscopy

Pablo D. Garcia[1] and Ricardo Garcia[1,*]
[1]Materials Science Factory Instituto de Ciencia de Materiales de Madrid, CSIC, Madrid, Spain

ABSTRACT The elastic response of a living cell is affected by its physiological state. This property provides mechanical fingerprints of a cell's dysfunctionality. The softness (kilopascal range) and thickness (2–15 μm) of mammalian cells imply that the force exerted by the probe might be affected by the stiffness of the solid support. This observation makes infinite sample thickness models unsuitable to describe quantitatively the forces and deformations on a cell. Here, we report a general theory to determine the true Young's moduli of a single cell from a force-indentation curve. Analytical expressions are deduced for common geometries such as flat punches, paraboloids, cones, needles, and nanowires. For a given cell and indentation, the influence of the solid support on the measurements is reduced by using sharp and high aspect ratio tips. The theory is validated by finite element simulations.

INTRODUCTION

The atomic force microscope (AFM) provides a variety of approaches to determine the mechanical properties and interactions of living cells (1–3). In particular, the elastic moduli of cells have been extensively measured (4–17) because of their relationship to the physiological and pathological state of the cell (1,4,18–20). This observation has led to a variety of AFM measurements to distinguish cells in a variety of diseases (21–30). The implications of force spectroscopy measurements on mechanotransduction processes and their potential for diagnostics have raised a variety of questions. Those concerns include fundamental aspects such as the contact mechanics model to describe the cell's deformation (5,31–33), the linearity of the mechanical response (5,7,14,33), the influence of the probe's dynamics (34), or the interplay between elastic, viscoelastic, and energy dissipation processes (35–38). Relevant experimental issues are focused on the determination of the contact point (39), the calibration of the probe's force constant (40,41), or the influence of the hydrodynamic drag of the cantilever on the force measured by the AFM (42,43).

The most fundamental and longstanding issue is the choice of the contact mechanics model needed to transform force-indentation curves into elastic moduli. Contact mechanics models based on Hertz, Boussinesq, or Sneddon (44–46) theories are routinely applied in cell nanomechanics (1,4,6,7,9–11,20–24,29,41). Those models provide analytical expressions that relate the Young's modulus, indentation, and force (45–47). A key assumption in the calculations is to consider the sample with an infinite thickness. Semi-infinite contact mechanics models neglect the influence of the stiffness of the substrate used to culture the cell on the determination of the elastic properties. This assumption might introduce significant errors in the determination of the Young's modulus of a cell (8). In fact, this concern has been considered in macroscopic measurements performed on thick layers (48) years before the invention of the AFM and its application to cell nanomechanics.

In an AFM experiment, the stress applied by the probe could propagate through the cell to reach the substrate and then be reflected back to the cell's surface and modify the cantilever's deflection. This effect could be a major source of quantitative errors in the determination of the Young's modulus of a cell. There are several factors that make this effect more relevant on living cells than in any other finite soft sample. First, the cell's thickness is in the 2–10 μm range, whereas a typical AFM experiment generates indentations between 200 nm and 2 μm, that is, ~20% of the cell's thickness. Second, typical Young's moduli values for mammalian cells are in the kilopascal range, that is, ~8 orders of magnitude smaller than the Young's modulus of the glass substrate supporting the cells.

Several years ago, Dimitriadis et al. discussed the influence of the substrate on the cell's elastic properties as measured by a spherical AFM probe (5). This effect was later described as the bottom effect artifact (8). Dimitriadis's theory enables us to determine the force exerted by a spherical tip on a cell as a function of the indentation (5). The theory provides an expression to determine the Young's modulus without the influence of the solid support.

The bottom effect correction proposed by Dimitriadis et al. has three limitations. First, this approach is hard to generalize to other relevant geometries. Second, the method has not been validated by numerical simulations and/or other theories. Third, it treats the variation of the contact area with the indentation as in a Hertzian contact.

Here, we present a general theory to determine the elastic moduli in a force-indentation experiment of a thin soft layer, in particular, a living cell attached to a solid support. We show that the forces measured by AFM on cells are affected by the solid support. This effect is unavoidable in force microscopy. It is a consequence of some cellular properties such as finite thickness, softness, and incompressibility. We show that the bottom effect artifact is controlled by the ratio between the contact radius and the cell thickness, and we also show how this ratio changes with the indentation. The bottom effect elastic theory describes the above features while enabling the determination of the true elastic modulus of the cell without the influence of the solid support.

The theory is valid for any axisymmetric tip shape, in particular spherical, conical, flat punches, needles, and nanowires. The theory provides the force as a function of the indentation and contact radius as a sum of terms expressed in powers of the inverse of the sample thickness. We show that those expressions converge when the number of terms used in the approximation is increased. We also show that the theory matches the forces and deformations given by finite element simulations.

MATERIALS AND METHODS

Theory of the forces and deformations of a thin sample on top of rigid support

Fig. 1 a illustrates a force microscopy-cell interface. Fig. 1 b shows the dependence of the force exerted on a cell (theory) as a function of the indentation for a sinusoidal modulation of the tip-cell distance.

Let us consider an axisymmetric probe that applies a force on a soft sample of thickness h deposited on the xy plane. The sample rests on rigid support. The axial deformation u_z along the direction perpendicular to the xy plane on a point (x_0, y_0) can be expressed in terms of the pressure distribution P_z and the Green's function G as follows (5,49):

$$u_z(x_0, y_0) = \iint P_z(x, y) G(\rho) dA. \qquad (1)$$

The $G(\rho)$ function represents the displacement profile generated by a point force applied on a surface point (x, y) at a distance $\rho =$
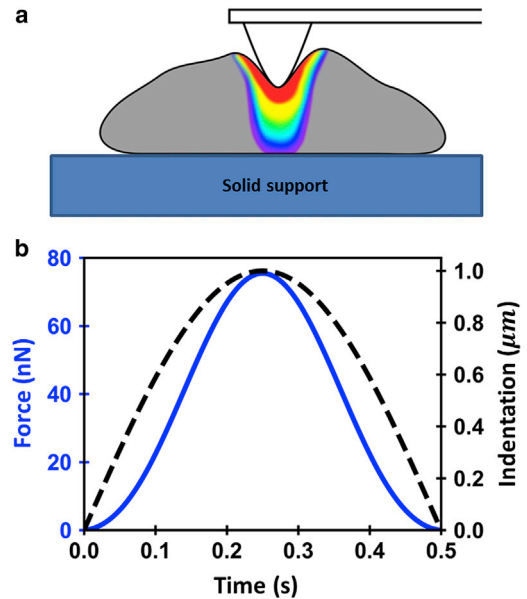
FIGURE 1 (a) Scheme of the probe cell-solid support interface in a force spectroscopy measurement. The changes in color provide a qualitative indication of the stress variation across the interface (stress from *high* to *low*, *red>yellow>green>blue*). (b) The probe's displacement (*black*) and probe-cell force (*blue*) are shown as a function of time for a sinusoidal modulation of $A = 1~\mu m$ and $f_m = 1$ Hz. Other data include $E_{cell} = 4$ kPa, $h = 2.5~\mu m$, and $R = 5~\mu m$. To see this figure in color, go online.

$\sqrt{(x - x_0)^2 + (y - y_0)^2}$; dA is an element of the area of the contact region. Dimitriadis et al. (5) showed that the G function of a finite sample could be expressed as the Taylor series of the ratio ε between the indentation at the center of the contact area δ (it coincides with the maximal indentation) and the sample thickness h ($\varepsilon = \delta/h$) as follows:

$$G(\rho) = G_0(\rho) \left[1 + \alpha_0 \frac{\rho}{\delta} \varepsilon + \beta_0 \frac{\rho^3}{\delta^3} \varepsilon^3 + \dots \right], \qquad (2)$$

where G_0 is the Green function of a semi-infinite sample with the same intensive mechanical properties as the finite sample. For a probe of shape $f(r)$, the deformation on a point inside the area of contact is given by

$$u_z(x_0, y_0) = \delta - f(r_0), \qquad (3)$$

with $r_0 = \sqrt{x_0^2 + y_0^2}$. Then, the pressure profile can be expressed in terms of a Taylor series as follows:

$$P = P_0 + P_1\varepsilon + P_2\varepsilon^2 + P_3\varepsilon^3 + P_4\varepsilon^4 + \mathcal{R}(\varepsilon^5). \qquad (4)$$

The first-order term P_0 represents the pressure profile exerted by the same probe on a semi-infinite sample. The P_n terms are the solutions of integral equations (see Supporting Materials and Methods). Once these integrals are solved, the force exerted on the cell could be recovered by integrating the pressure profile within the contact region as follows:

$$F = \iint P_z(x, y) dA. \qquad (5)$$

A flat-ended cylindrical probe (flat punch) provides a geometry that facilitates the solution of the integral equations to determine the force

profiles. It represents our reference geometry for the calculations of the next sections. For that reason, we provide the analytical expression of the P_n components for the flat punch (see Supporting Materials and Methods):

$$P_0 = \frac{E\delta}{\pi(1-\nu^2)}(a-r^2)^{-\frac{1}{2}}, \tag{6a}$$

$$P_1 = -P_0\frac{2a\alpha_0}{\pi}\frac{1}{\delta}, \tag{6b}$$

$$P_2 = P_0\left(\frac{2a\alpha_0}{\pi}\frac{1}{\delta}\right)^2, \tag{6c}$$

$$P_3 = -\frac{8a^3 E}{\pi^2(1-\nu^2)\delta^2}\left(\frac{\alpha_0^3}{\pi^2}-\frac{\beta_0}{3}+\frac{\beta_0 r^2}{a^2}\right)(a-r^2)^{-\frac{1}{2}}, \tag{6d}$$

and

$$P_4 = \frac{16a^4 E}{\pi^5(1-\nu^2)\delta^3}\left(\alpha_0^4+\frac{\alpha_0\beta_0\pi^2 r^2}{a^2}\right)(a-r^2)^{-\frac{1}{2}}, \tag{6e}$$

where a is the radius of the punch, E is the Young's modulus of the sample, and ν is the Poisson coefficient. α_0 and β_0 are numerical parameters that depend on the type of attachment of the sample to the rigid substrate and the Poisson coefficient (5,31). For $r = \sqrt{x^2+y^2} > a$ (that is, outside the contact region), P_n values are zero.

Determining the force by applying Eq. 5 for other geometries might be very demanding. In general, the integral equations leading to P_n are hard to solve. For some geometries, the integrals might not have analytical solutions. In addition, the direct approach cannot be generalized. A change of the probe's geometry involves solving a new set of integral equations. For those reasons, we implement an alternative method that is equivalent to the direct approach but is mathematically more manageable. This method is applicable for any axisymmetric tip.

Bottom effect elastic theory to determine the force exerted by an axisymmetric probe

The method combines the reciprocal theorem for linear elastic solids and the determination of the pressure profile exerted by a flat punch. The reciprocal theorem developed independently by Betti, Maxwell, and Raleigh (50) establishes an equivalence between the work performed by two different pressure fields on the same sample, such as the ones generated by two different AFM probes.

Let us consider a linear elastic body of arbitrary shape. The application of a field of pressures $P_i(x_j)$ on the surface of the body will generate a field of deformations $u_i(x_j)$, where x_j represents the spatial coordinate in the xyz space in which the deformation is calculated. If we apply a different field of pressures $P^*_i(x_j)$, for example, by using a probe with a different geometry, we will obtain a different field of deformations $u^*_i(x_j)$. The reciprocal theorem establishes the following equivalence:

$$\iint P_i u^*_i dA = \iint P^*_i u_i dA, \tag{7}$$

where the integral is performed over the whole surface of the body. As a reference probe, we use the flat punch because we have already deduced the analytical expressions of the pressure distribution and the deformation. In Eq. 7, the only unknown is the field of pressures P_z. The deformations u_z across the contact region are determined from the probe shape.

To simplify the mathematical derivation, we assume that all the forces exerted on the sample surface are applied parallel to the vertical axis z; thus, the lateral components of the pressure are zero:

$$P_x(x_i) = P_y(x_i) = P^*_x(x_i) = P^*_y(x_i) = 0. \tag{8}$$

Let us apply the reciprocal theorem for an axisymmetric probe of geometry $f(r)$ and the flat punch ($f_{punch}(r) = 0$) (see Supporting Materials and Methods) as follows:

$$2\pi\int_0^a P_z(r)\delta^* r dr = 2\pi\int_0^{a^*} P^*_z(r)[\delta - f(r)]r dr, \tag{9}$$

which leads to an expression of the force exerted on the sample in terms of the maximal indentation and the contact area $F(\delta,a)$:

$$F = \frac{2\pi}{\delta^*}\int_0^a P^*_z(r)[\delta - f(r)]r dr. \tag{10}$$

We have assumed that the maximal indentation δ and the contact radius a are identical for the reference and problem probes. We note that with independence of the probe geometry, there is a flat punch that will satisfy the above conditions.

Force-indentation equations for flat punch, paraboloid, and conical probes

To obtain the force as a function of the indentation on a single cell, we need to define the geometry of the indenter, include the cell's incompressibility (Poisson coefficient $\nu_{cell} = 0.5$), set some boundary conditions such as type of cell attachment to the solid support, and determine the dependence of the contact area as a function of the indentation (finite thickness). The latter is obtained by solving the following (51):

$$\frac{\partial F(\delta, a)}{\partial a} = 0. \tag{11}$$

The mathematics to solve the integral of Eq. 10 for the different geometries involves several intermediate steps (Supporting Materials and Methods). The intermediate expressions are valid to describe the forces and deformation of any sample of finite thickness on top of solid support. The particularization for a cell comes from the introduction of the boundary conditions and the cell's Poisson coefficient.

RESULTS

Flat punch

The contact area for a flat-ended cylindrical punch does not depend on the indentation ($f(r) = 0$). By inserting Eq. 6 into Eq. 10, the attachment of the cell to the solid support (boundary condition), and $\nu_{cell} = 0.5$, we obtain the following expression of the force on the cell as a function of the indentation, cell thickness, and Young's modulus:

$$F_{punch} = F_0\left[\frac{1}{h^0}+\frac{1.133a}{h}+\frac{1.283a^2}{h^2}+\frac{0.598a^3}{h^3}\right.$$
$$\left.-\frac{0.291a^4}{h^4}\right], \tag{12a}$$

with

$$F_0 = \frac{8a}{3}E_{cell}\delta, \tag{12b}$$

where F_0 represents the force exerted on a semi-infinite sample. Equation 12 *a* reveals that the force scales with the contact area and the sample thickness. It underlines a counterintuitive result: for a flat punch, the F/F_0 ratio does not depend on the indentation value. The key factor is the dependence of the a/h ratio on δ.

Conical probe

The shape of a conical probe of semiangle θ is given by

$$f(r) = \frac{r}{\tan\theta}. \tag{13}$$

The application of the reciprocal theorem and boundary conditions leads to

$$F_{cone} = F_0\left[\frac{1}{h^0} + \frac{0.721\delta\tan\theta}{h} + \frac{0.650\delta^2\tan^2\theta}{h^2}\right.$$
$$\left. + \frac{0.491\delta^3\tan^3\theta}{h^3} + \frac{0.225\delta^4\tan^4\theta}{h^4}\right], \tag{14a}$$

with

$$F_0 = \frac{8\tan\theta}{3\pi}E_{cell}\delta^2. \tag{14b}$$

Paraboloid

In the case of a paraboloid, the shape of the probe is

$$f(r) = \frac{r^2}{2R}. \tag{15}$$

Then, the force can be expressed as

$$F_{sphere} = F_0\left[\frac{1}{h^0} + \frac{1.133\sqrt{\delta R}}{h} + \frac{1.497\delta R}{h^2} + \frac{1.469\delta R\sqrt{\delta R}}{h^3}\right.$$
$$\left. + \frac{0.755\left(\delta^2 R^2\right)}{h^4}\right], \tag{16a}$$

with

$$F_0 = \frac{16}{9}E_{cell}\sqrt{R}\delta^{3/2}. \tag{16b}$$

The above expression can only be applied for $\delta \leq R$; for that reason, we call it F_{sphere}. This expression resembles the one deduced by Dimitriadis et al. (5), but the coefficients
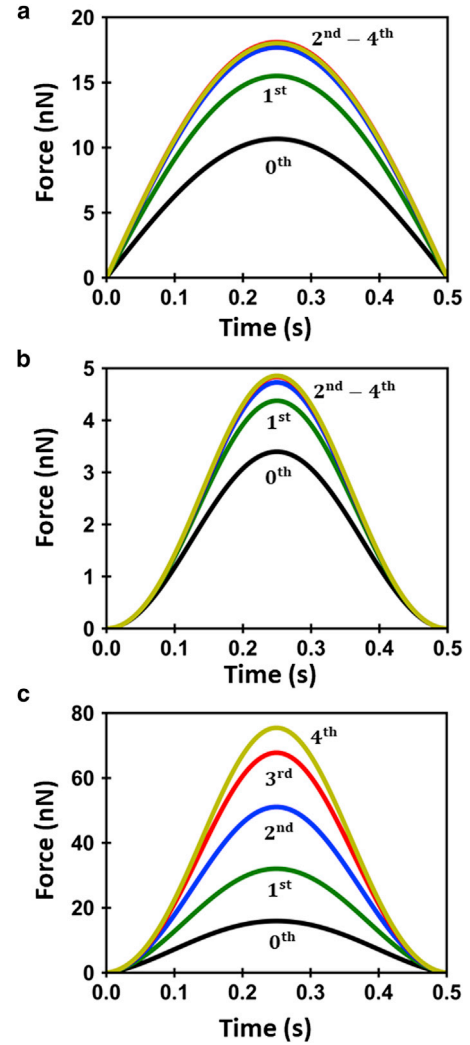
FIGURE 2 Bottom effect elastic corrections as a function of the approximation order. (*a*) Force is shown as a function of time for a flat punch with a radius of $a = 1~\mu m$. The force curves for the second-, third-, and fourth-order approximations are very similar. (*b*) Force is shown as a function of time for a conical tip with a semiangle $\theta = 45°$. (*c*) Force is shown as a function of time for a parabolic tip of $R = 5~\mu m$. The numbers indicate that the force is calculated by adding the terms until that order, for example, for a conical indenter, $F_{cone}(0th) = F_0 = F_{Sneddon\text{-}cone}$, $F_{cone}(1st) = F_0 + F_1$, $F_{cone}(2nd) = F_0 + F_1 + F_2$ and so on. Other data include $E_{cell} = 4$ kPa, $h = 2.5~\mu m$; $A = 1~\mu m$ and $f_m = 1$ Hz. To see this figure in color, go online.

that multiply the terms $1/h^n$ are different. We have used a non-Hertzian model to express the change of the contact area with the indentation, whereas in (5), the contact area was calculated by using Hertz contact mechanics. Because of that approximation, the Dimitriadis et al. (5) expression underestimates the force applied on the cell (see FS3 in Supporting Materials and Methods).

Force-indentation equations for other axisymmetric probes: needles and nanowires

The same procedure has been applied to deduce the force as a function of the cell properties, indentation, and probe
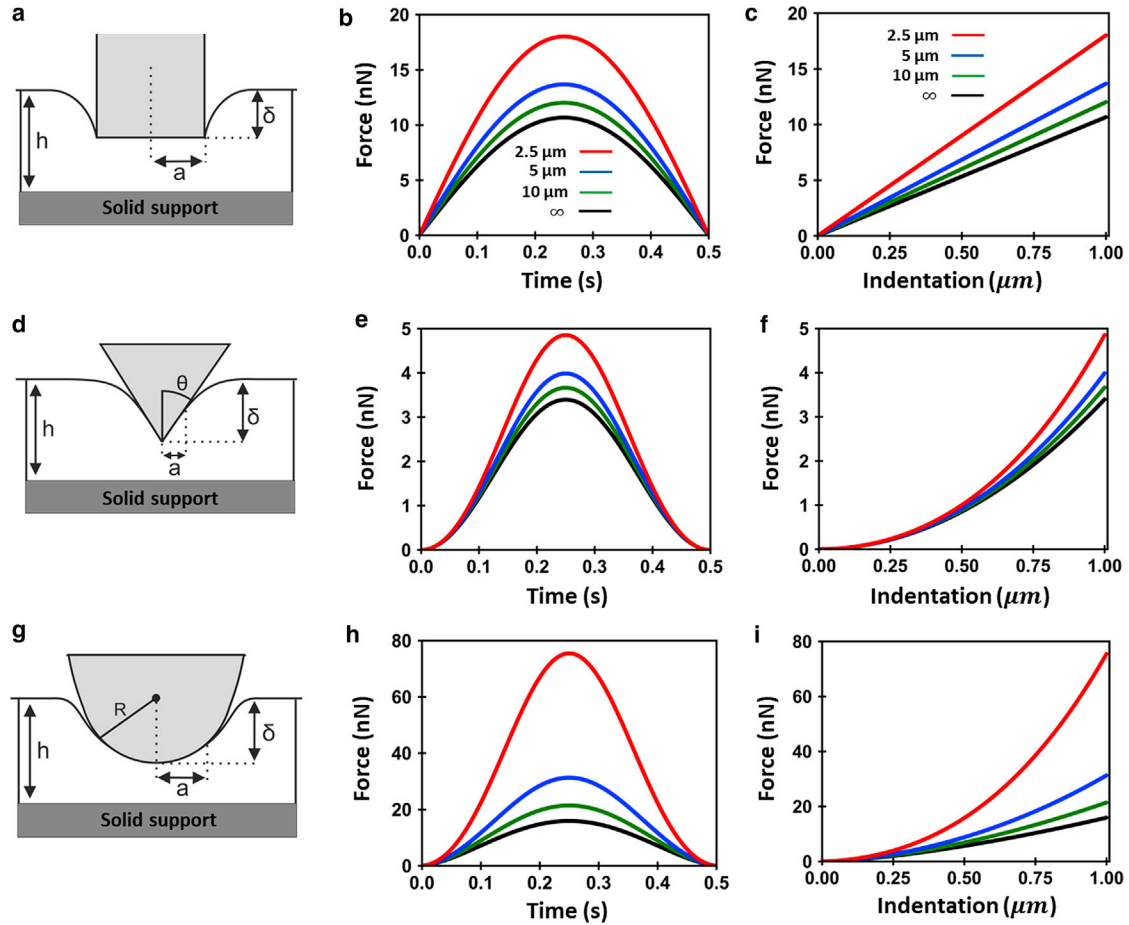
FIGURE 3 Force curves as a function of the sample thickness. The force is plotted as a function of time and indentation for flat punch, parabolic, and conical probes. (*a*) A side view is shown of the flat punch cell-solid support interface. (*b*) The force-time curve is shown for a flat punch (*a* = 1 μm). (*c*) The force-indentation curve is shown for a flat punch (*a* = 1 μm). (*d*) A side view is shown of the cone cell-solid support interface. (*e*) A force-time curve is shown for a cone (semiangle *θ* = 45°). (*f*) The force is shown as a function of indentation exerted by a cone (*θ* = 45°). (*g*) A side view is shown of the paraboloid cell-solid support interface. (*h*) The force-time curve for a parabolic tip (*R* = 5 μm) is shown. (*i*) The force-indentation curve is shown for a parabolic tip (*R* = 5 μm). The force curves have been calculated with fourth-order approximation. Sinusoidal modulation of *A* = 1 μm and *f*$_m$ = 1 Hz, *E*$_{cell}$ = 4 kPa is shown. The thickness of the sample, from top to bottom, is 2.5, 5, and 10 μm and semi-infinite. To see this figure in color, go online.

geometry for other axisymmetric tips. In particular, we have deduced the force-indentation equations for two of the more interesting probes for mapping nanomechanical properties at high spatial resolution, needles, and nanowires. For example, a nanowire is approximated by a flat punch capped with a hemisphere. The force for a nanowire is derived from the flat punch and paraboloid equations by introducing a critical indentation δ_c. This indentation defines the value at which the contact radius coincides with the radius R of the probe:

$$F_{nw}(\delta) = \begin{cases} F_{sphere}(\delta) & if\ \delta \leq \delta_c \\ F_{sphere}(\delta_c) + F_{punch}(\delta - \delta_c) & if\ \delta > \delta_c \end{cases}.$$
(17)

A needle is approximated by a flat punch capped with a cone:

$$F_{needle}(\delta) = \begin{cases} F_{cone}(\delta) & if\ \delta \leq \delta_c \\ F_{cone}(\delta_c) + F_{punch}(\delta - \delta_c) & if\ \delta > \delta_c \end{cases}.$$
(18)

DISCUSSION

Consistency of the bottom effect elastic theory

Fig. 2 illustrates the dependence of the force exerted on a cell as a function of time for a tip-cell distance modulation given by

$$d = A \sin(2\pi f_m t).$$
(19)

The force in Eqs. 12, 14, and 16 is expressed as a sum of terms (1/*h*^{n}). The term corresponding to *n* = 0 represents a sample with infinite thickness. It coincides with the

expressions provided by Sneddon (44) for paraboloid, cone, and flat punch geometries. We note that Hertz contact mechanics is a particular case of Sneddon's theory. We have verified that the results described in the following sections are valid for other types of tip-cell distance modulations, in particular, for triangular waveforms.

Fig. 2 shows that for those geometries, the force converges as the order of the polynomial is increased. This result represents an internal validation of the theory. We note that a previous attempt to deduce the force exerted by a conical tip on a cell did not converge, as more terms were included in the calculation of the force (8) (see FS4 in the Supporting Materials and Methods).

Force curves as a function of the cell thickness

We have calculated the dependence of the force exerted on a cell as a function of its thickness for an indentation of 1 μm for flat punch, conical, and parabolic probes (Fig. 3). The cell is simulated with parameters $E_{cell} = 4$ kPa, $\nu = 0.5$. We have considered three values of the cell thickness: 2.5, 5, and 10 μm. Those values represent the thicknesses across different regions of a cell: 2.5 μm near the edges, 5 μm near the nucleus, and 10 μm on top of the nucleus. We have also plotted the results for a semi-infinite sample. To provide a complete characterization of these effects, the force is plotted as a function of time and indentation.

The force increases as the sample thickness is decreased. This observation is an unavoidable consequence of three factors: the cell's Poisson coefficient, thickness (1–15 μm), and very small Young's modulus (0.5–10 kPa). The results illustrate the influence of the stiffness of the substrate on force spectroscopy measurements. The bottom effect elastic corrections decrease as the thickness sample (cell) is increased.

Fig. 4 shows the competition between the bottom effect, the indentation, and the contact area in the measured force. Force distance and time curves are calculated as a function of the probe's radii for a nanowire. To visualize the bottom effect contribution, we have calculated the force exerted by the same probe on a semi-infinite sample (discontinuous curves). The bottom effect plays a major factor in the determination of the force whenever the contact radius and sample thickness are within the same order of magnitude. In cell nanomechanics, the use of sharp and high-aspect ratio probes significantly reduces the influence of the solid support in the determination of the force.

Comparison between bottom effect corrections and finite element simulations

To test the validity of the above expressions, we have compared them with finite element method (FEM) simula-
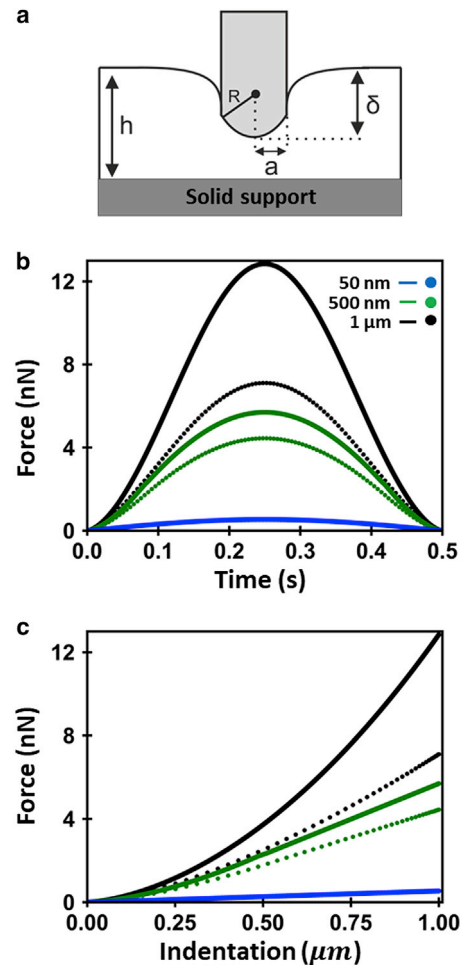
FIGURE 4 Force curves for nanowire probes. (*a*) A side view is shown of the nanowire cell-solid support interface. (*b*) The force-time curve is shown for nanowires of $R = 1$ μm, and 500 and 50 nm. (*c*) A force-indentation curve is shown for different nanowires. The discontinuous lines show the force curves obtained for the same probe applying a force on a semi-infinite sample. For the sharpest tip, the force curves given by the semi-infinite model and the bottom effect elastic theory are nearly identical. Layer parameters include $E_{cell} = 4$ kPa, $h = 2.5$ μm, and semi-infinite $E_{cell} = 4$ kPa. To see this figure in color, go online.

tions. In this comparison, the results provided by the FEM simulations are considered to provide the "true" behavior of a linear elastic and homogeneous material. The numerical simulations were performed by using the COMSOL software (COMSOL Multiphysics; COMSOL AB, Stockholm, Sweden).

Fig. 5 shows three of the interfaces simulated by FEM. The interface is formed by the probe, a finite elastic layer attached to a rigid support. The interfaces for a flat punch (Fig. 5 *a*), cone (Fig. 5 *b*), and paraboloid of radius R (Fig. 5 *c*) are shown. In the FEM simulations, the probe is considered an isotropic and homogeneous elastic material characterized by a Young's modulus of 20 GPa. The layer is simulated by a cylinder of length and radius, respectively, of 5 and 50 μm. For completeness, we have also simulated
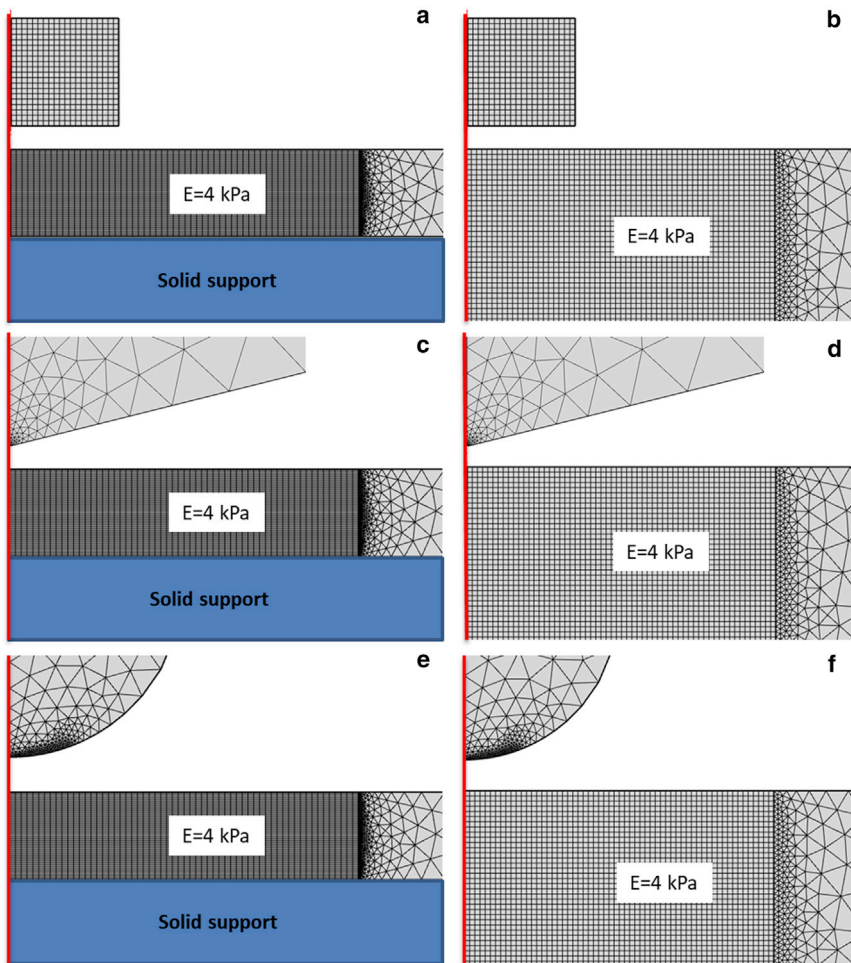
FIGURE 5 Finite element interfaces. (*a*) The FEM scheme is shown of the interface formed by a flat punch on top of finite elastic layer deposited on rigid solid support. (*b*) The FEM scheme is shown of a flat punch on top of a semi-infinite linear elastic sample. (*c*) The FEM scheme is shown of the interface formed by a conical tip on top of finite elastic sample deposited on rigid solid support. (*d*) The FEM scheme is shown of a conical tip on top of a semi-infinite linear elastic sample. (*e*) The FEM scheme is shown of the interface formed by a parabolic tip on top of finite elastic sample deposited on rigid solid support. (*f*) The FEM scheme is shown of a parabolic tip on top of a semi-infinite elastic sample. The sample is either finite or semi-infinite and has $E_{cell} = 4$ kPa. The simulated systems have cylindrical symmetry around the vertical axis (*red line*). To see this figure in color, go online.

the response of a semi-infinite material. In this case, the semi-infinite material is approximated by a thick layer with length and radius, respectively, of 50 and 50 μm. The boundary condition for the rigid support implies zero displacements in the in- and out-plane directions. The tip-layer distance was modulated by a sinusoidal waveform with a frequency of $f_m = 1$ Hz.

The simulations generate what we consider the true force-indentation curves. Those curves are compared with the forces given, respectively, by Eqs. 12, 14, and 16. From the fittings, we deduce the Young's moduli of the finite layer. Those values are compared to the ones introduced in the FEM simulations.

Fig. 6 shows the dependence of the Young's moduli as a function of the indentation/thickness ratio for a sample of thickness $h = 5$ μm. The bottom effect elastic theory enables us to recover the Young's modulus for the three interfaces. The determination of the Young's modulus provided by the bottom effect theory does not depend on the indentation ratio (Fig. 6). This result is in sharp contrast with the values provided by Sneddon contact mechanics. Sneddon contact mechanics (Hertz's included) significantly overes-

timate the value of the Young's moduli. The overestimation increases with the indentation for conical (Fig. 6 *b*) and parabolic tips (Fig. 6 *c*), whereas it remains flat for a punch (Fig. 6 *a*). This happens because the contact area for parabolic and conical tips shows a rapid increase with the indentation. The flat punch represents the opposite case; the contact area does not change with the indentation. As a consequence, the error in the determination of the Young's modulus by using the semi-infinite model does not depend on the indentation (Fig. 6 *a*). The above results illustrate a remarkable property of the bottom effect artifact. On a given cell, the influence of the substrate stiffness increases with the contact area and thus with the size of the probe.

The FEM simulations have been performed by assuming that the surface of sample that is in physical contact with the probe does not have lateral displacements. Those displacements happen in the regions of the sample underneath the contact area. In Supporting Materials and Methods, we present the results obtained for a boundary condition that allows lateral displacements in the surface of the cell in contact with the probe.
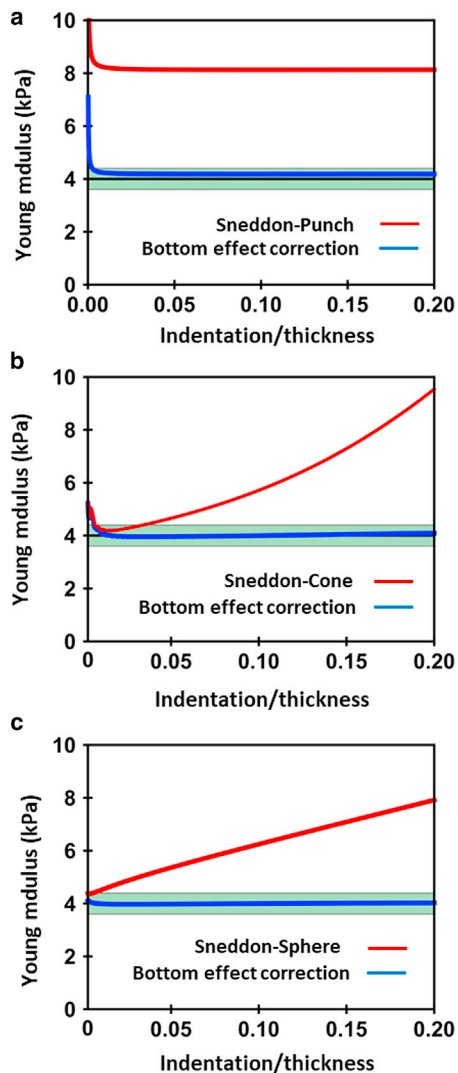
FIGURE 6 Determination of the Young's modulus from the bottom effect theory and Sneddon contact mechanics. (*a*) Flat punch of *a* = 2.5 *μ*m is shown. (*b*) Conical tip of *θ* = 76° is shown. (*c*) Parabolic tip of *R* = 5 *μ*m is shown. The elastic moduli determined by the bottom effect (*blue line*) and infinite thickness theories (*red line*) are plotted as a function of the indentation/thickness ratio (*h* = 5 *μ*m). The bottom effect elastic corrections have been calculated by using the fourth-order approximation. The force-distance curves have been generated by FEM simulations for a 5-*μ*m-thick sample with a Young's modulus of 4 kPa. The curves are fitted with the expressions for the flat punch, cone, and parabolic tips. The *green* stripe shows the values that lie within a 10% window from the Young's modulus of the sample (4 kPa). To see this figure in color, go online.

The use of large colloidal tips (41,52) with radii of several micrometers has been recommended to determine the Young's moduli of living cells (7,41). Those probes provide a uniform and well-defined shape during the interaction with the cell. The above results show that the determination of the Young's moduli with those probes makes unavoidable the use of a bottom effect elastic theory; otherwise, the accuracy of the Young's moduli provided by force spectroscopy measurements is highly questionable.

CONCLUSIONS

The force exerted by a probe on a living cell is influenced by the stiffness of the solid support. We have developed a bottom effect elastic theory to describe the forces and deformations exerted by a probe on an adherent cell deposited on rigid support. The theory provides analytical expressions to determine the force as a function of the thickness of the sample, the indentation, and the contact area. The theory shows that the force exerted on a cell is augmented by the presence of the solid support. This result is an unavoidable consequence of the boundary conditions existing in an AFM experiment. Despite this effect, the bottom effect elastic theory enables recovery of the intrinsic mechanical properties of the cell such as the Young's modulus with independence of the stiffness of the solid support. The bottom effect elastic corrections decrease as the contact area between the probe and the cell is reduced. This leads to a counterintuitive result; for a given cell, the use of sharper tips reduces the bottom effect artifact.

The theory is general. It can be extended to the geometry of any axisymmetric tip. Specifically, we have deduced analytical expressions for flat punch, conical, paraboloid, needle, and nanowire probes. The theory has been validated by using FEM simulations.

SUPPORTING MATERIAL

Supporting Materials and Methods and four figures are available at http://www.biophysj.org/biophysj/supplemental/S0006-3495(18)30590-3.

AUTHOR CONTRIBUTIONS

P.D.G. developed the theory and performed the numerical simulations. R.G. conceived the project and supervised the theory and simulations. R.G. wrote the article. P.D.G. and R.G. analyzed the data, discussed the results, and revised the article.

REFERENCES

1. Dufrêne, Y. F., T. Ando, …, D. J. Müller. 2017. Imaging modes of atomic force microscopy for application in molecular and cell biology. *Nat. Nanotechnol.* 12:295–307.

2. Alsteens, D., R. Newton, …, D. J. Müller. 2017. Nanomechanical mapping of first binding steps of a virus to animal cells. *Nat. Nanotechnol.* 12:177–183.

3. Helenius, J., C. P. Heisenberg, …, D. J. Muller. 2008. Single-cell force spectroscopy. *J. Cell Sci.* 121:1785–1791.

4. Rotsch, C., and M. Radmacher. 2000. Drug-induced changes of cytoskeletal structure and mechanics in fibroblasts: an atomic force microscopy study. *Biophys. J.* 78:520–535.

5. Dimitriadis, E. K., F. Horkay, …, R. S. Chadwick. 2002. Determination of elastic moduli of thin layers of soft material using the atomic force microscope. *Biophys. J.* 82:2798–2810.

6. Roduit, C., S. Sekatski, …, S. Kasas. 2009. Stiffness tomography by atomic force microscopy. *Biophys. J.* 97:674–677.

7. Harris, A. R., and G. T. Charras. 2011. Experimental validation of atomic force microscopy-based cell elasticity measurements. *Nanotechnology.* 22:345102.

8. Gavara, N., and R. S. Chadwick. 2012. Determination of the elastic moduli of thin samples and adherent cells using conical atomic force microscope tips. *Nat. Nanotechnol.* 7:733–736.

9. Vargas-Pinto, R., H. Gong, …, M. Johnson. 2013. The effect of the endothelial cell cortex on atomic force microscopy measurements. *Biophys. J.* 105:300–309.

10. Liu, H., J. Wen, …, Y. Sun. 2014. In situ mechanical characterization of the cell nucleus by atomic force microscopy. *ACS Nano.* 8:3821–3828.

11. Braunsmann, C., J. Seifert, …, T. E. Schäffer. 2014. High-speed force mapping on living cells with a small cantilever atomic force microscope. *Rev. Sci. Instrum.* 85:073703.

12. Guz, N., M. Dokukin, …, I. Sokolov. 2014. If cell mechanics can be described by elastic modulus: study of different models and probes used in indentation experiments. *Biophys. J.* 107:564–575.

13. Rigato, A., F. Rico, …, S. Scheuring. 2015. Atomic force microscopy mechanical mapping of micropatterned cells shows adhesion geometry-dependent mechanical response on local and global scales. *ACS Nano.* 9:5846–5856.

14. Valero, C., B. Navarro, …, J. M. García-Aznar. 2016. Finite element simulation for the mechanical characterization of soft biological materials by atomic force microscopy. *J. Mech. Behav. Biomed. Mater.* 62:222–235.

15. Wang, A., K. Vijayraghavan, …, M. J. Butte. 2016. Fast stiffness mapping of cells using high-bandwidth atomic force microscopy. *ACS Nano.* 10:257–264.

16. Cartagena-Rivera, A. X., C. M. Van Itallie, …, R. S. Chadwick. 2017. Apical surface supracellular mechanical properties in polarized epithelium using noninvasive acoustic force spectroscopy. *Nat. Commun.* 8:1030.

17. Beicker, K., E. T. O'Brien, III, …, R. Superfine. 2018. Vertical light sheet enhanced side-view imaging for AFM cell mechanics studies. *Sci. Rep.* 8:1504.

18. Lekka, M., P. Laidler, …, A. Z. Hrynkiewicz. 1999. Elasticity of normal and cancerous human bladder cells studied by scanning force microscopy. *Eur. Biophys. J.* 28:312–316.

19. Fuhrmann, A., J. R. Staunton, …, R. Ros. 2011. AFM stiffness nanotomography of normal, metaplastic and dysplastic human esophageal cells. *Phys. Biol.* 8:015007.

20. Moeendarbary, E., L. Valon, …, G. T. Charras. 2013. The cytoplasm of living cells behaves as a poroelastic material. *Nat. Mater.* 12:253–261.

21. Cross, S. E., Y. S. Jin, …, J. K. Gimzewski. 2007. Nanomechanical analysis of cells from cancer patients. *Nat. Nanotechnol.* 2:780–783.

22. Lekka, M., K. Pogoda, …, Z. Stachura. 2012. Cancer cell recognition–mechanical phenotype. *Micron.* 43:1259–1266.

23. Ramos, J. R., J. Pabijan, …, M. Lekka. 2014. The softening of human bladder cancer cells happens at an early stage of the malignancy process. *Beilstein J. Nanotechnol.* 5:447–457.

24. Calzado-Martín, A., M. Encinar, …, A. San Paulo. 2016. Effect of actin organization on the stiffness of living breast cancer cells revealed by peak-force modulation atomic force microscopy. *ACS Nano.* 10:3365–3374.

25. Staunton, J. R., B. L. Doss, …, R. Ros. 2016. Correlating confocal microscopy and atomic force indentation reveals metastatic cancer cells stiffen during invasion into collagen I matrices. *Sci. Rep.* 6:19686.

26. Karsch, S., D. Kong, …, A. Janshoff. 2017. Single-cell defects cause a long-range mechanical response in a confluent epithelial cell layer. *Biophys. J.* 113:2601–2608.

27. Rigato, A., A. Miyagi, …, F. Rico. 2017. High-frequency microrheology reveals cytoskeleton dynamics in living cells. *Nat. Phys.* 13:771–775.

28. Mohamed, M. S., A. Kobayashi, …, R. W. Wong. 2017. High-speed atomic force microscopy reveals loss of nuclear pore resilience as a dying code in colorectal cancer cells. *ACS Nano.* 11:5567–5578.

29. Schierbaum, N., J. Rheinlaender, and T. E. Schäffer. 2017. Viscoelastic properties of normal and cancerous human breast cells are affected differently by contact to adjacent cells. *Acta Biomater.* 55:239–248.

30. Tavares, S., A. F. Vieira, …, F. Janody. 2017. Actin stress fiber organization promotes cell stiffening and proliferation of pre-invasive breast cancer cells. *Nat. Commun.* 8:15237.

31. Chadwick, R. 2002. Axisymmetric indentation of a thin incompressible elastic layer. *SIAM J. Appl. Math.* 62:1520–1530.

32. Managuli, V., and S. Roy. 2017. Simultaneous analysis of elastic and nonspecific adhesive properties of thin sample and biological cell considering bottom substrate effect. *J. Biomech. Eng.* 139:091008.

33. Ding, Y., G. K. Xu, and G. F. Wang. 2017. On the determination of elastic moduli of cells by AFM based indentation. *Sci. Rep.* 7:45575.

34. Amo, C. A., and R. Garcia. 2016. Fundamental high-speed limits in single-molecule, single-cell, and nanoscale force spectroscopies. *ACS Nano.* 10:7117–7124.

35. Rother, J., H. Nöding, …, A. Janshoff. 2014. Atomic force microscopy-based microrheology reveals significant differences in the viscoelastic response between malign and benign cell lines. *Open Biol.* 4:140046.

36. Garcia, P. D., C. R. Guerrero, and R. Garcia. 2017. Time-resolved nanomechanics of a single cell under the depolymerization of the cytoskeleton. *Nanoscale.* 9:12051–12059.

37. Cartagena-Rivera, A. X., W. H. Wang, …, A. Raman. 2015. Fast, multifrequency, and quantitative nanomechanical mapping of live cells using the atomic force microscope. *Sci. Rep.* 5:11692.

38. Efremov, Y. M., W. H. Wang, …, A. Raman. 2017. Measuring nanoscale viscoelastic parameters of cells directly from AFM force-displacement curves. *Sci. Rep.* 7:1541.

39. Gavara, N. 2016. Combined strategies for optimal detection of the contact point in AFM force-indentation curves obtained on thin samples and adherent cells. *Sci. Rep.* 6:21267.

40. Sader, J. E., J. Lu, and P. Mulvaney. 2014. Effect of cantilever geometry on the optical lever sensitivities and thermal noise method of the atomic force microscope. *Rev. Sci. Instrum.* 85:113702.

41. Schillers, H., C. Rianna, …, M. Radmacher. 2017. Standardized nanomechanical atomic force microscopy procedure (SNAP) for measuring soft and biological samples. *Sci. Rep.* 7:5117.

42. Liu, R., M. Roman, and G. Yang. 2010. Correction of the viscous drag induced errors in macromolecular manipulation experiments using atomic force microscope. *Rev. Sci. Instrum.* 81:063703.

43. Berthold, T., G. Benstetter, …, M. Nafría. 2017. Numerical study of hydrodynamic forces for AFM operations in liquid. *Scanning.* 2017:6286595.

44. Sneddon, I. N. 1965. The relation between load and penetration in the axisymmetric boussinesq problem for a punch of arbitrary profile. *Int. J. Eng. Sci.* 3:47–57.

45. Harding, J. W., and I. N. Sneddon. 1945. The elastic stresses produced by the indentation of the plane surface of a semi-infinite elastic solid by a rigid punch. *Math. Proc. Camb. Philos. Soc.* 41:16–26.

46. Johnson, K. L. 1985. Contact Mechanics. Cambridge University Press, Cambridge, UK.

47. Pharr, G. M., W. C. Oliver, and F. R. Brotzen. 2011. On the generality of the relationship among contact stiffness, contact area, and elastic modulus during indentation. *J. Mater. Res.* 7:613–617.

48. Dhaliwal, R. S., and I. S. Rau. 1970. The axisymmetric boussinesq problem for a thick elastic layer under a punch of arbitrary profile. *Int. J. Eng. Sci.* 8:843–856.

49. Landau, L. D., E. M. Lifshitz, …, L. P. Pitaevskii. 1986. Fundamental equations. Theory of Elasticity, Third Edition. Butterworth-Heinemann, pp. 1–37.

50. Charlton, T. M. 1960. A historical note on the reciprocal theorem and theory of statically indeterminate frameworks. *Nature.* 187:231.

51. Shield, R. T. 1967. Load-displacement relations for elastic bodies. *Z. Angew. Math. Phys.* 18:682–693.

52. Ducker, W. A., T. J. Senden, and R. M. Pashley. 1992. Measurement of forces in liquids using a force microscope. *Langmuir.* 8:1831–1836.